Computational study of the equilibrium geometry and anharmonic vibrational spectra of PbX2**NO and PbX2**ON (X=F, Cl, Br, I) complexes

Andrzej T Kowal

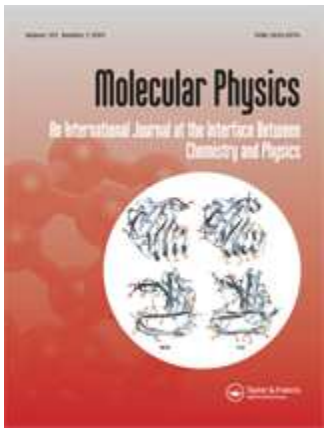

Computational study of the equilibrium geometry and anharmonic vibrational spectra of PbX2••NO and PbX2••ON (X=F, Cl, Br, I) complexes

Journal:	*Molecular Physics*
Manuscript ID:	TMPH-2010-0075.R1
Manuscript Type:	Full Paper
Date Submitted by the Author:	11-Apr-2010
Complete List of Authors:	Kowal, Andrzej; Wrocław University of Technology, Chemistry
Keywords:	lead(II) halide, anharmonic, effective core potential, VSCF, nitrogen monoxide

Computational study of the equilibrium geometry and anharmonic vibrational spectra of PbX_2··NO and PbX_2··ON (X=F, Cl, Br, I) complexes

Andrzej T. Kowal

Chemistry Department

Wrocław University of Technology, Wyb. St. Wyspiańskiego 27, 50-370 Wrocław, Poland

E-mail: andrzej.t.kowal@pwr.wroc.pl

Phone: +48 071 3203874

Fax: +48 071 3202441

Abstract

Equilibrium geometry parameters of the open shell PbX_2··NO and PbX_2··ON (X=F, Cl, Br, I) complexes have been computed by second-order Z-averaged perturbation theory (ZAPT2) with Stevens-Basch-Krauss-Jasien-Cundari (SBKJC) scalar-relativistic effective core potentials (RECP) and basis sets on all atoms. Equilibrium geometries of both PbX_2··NO and PbX_2··ON bonding isomers conform to C_s symmetry structure with end-on ligand coordination, and are characterized by Pb-N bond length within 266.6 – 271.7 pm range, Pb-O distance of 267.8 – 275.8 pm, Pb-N-O angle within 109.2 – 120.7 deg range, and Pb-O-N angle of 117.1 – 127.8 deg. Anharmonic vibrational spectra of the PbX_2··NO and PbX_2··ON complexes have been calculated by direct correlation-corrected vibrational self-consistent field (CC-VSCF) method enhanced with second-order perturbative correction using potential energy surfaces (PESs) determined at ZAPT2/SBKJC+(d) level in curvilinear (internal) coordinates. Fundamental of ν(Pb-N) stretching mode has been computed at 232.8 to 209.0 cm^{-1} within PbX_2··NO series whereas ν(Pb-O) stretching mode fundamental evaluation in PbX_2··ON series afforded wavenumbers within 183.2 – 150.7 cm^{-1} range. Blue shift of the ν(N=O) stretching mode wavenumber upon PbX_2··NO complex formation, computed in anharmonic approximation, 15.8 – 14.6 cm^{-1}, correctly reproduces the effect observed in the

low-temperature Ar matrix spectra of PbX_2··NO compounds. Influence of complex formation on the ν_s(Pb-X) and ν_{as}(Pb-X) fundamentals of PbX_2 halides has also been discussed. Two-dimensional mapping of the $V_{i,j}^{coup}(Q_i , Q_j)$ mode-mode coupling potential has been used to rationalize the origin of mode coupling related anharmonic corrections.

Key words: lead(II) halide, effective core potential, anharmonic, nitrogen monoxide

1. INTRODUCTION

Blue shift of the intra-ligand stretching mode of σ-donors like CO, NO and N_2, observed in the infrared spectra of fourth row divalent metal halides MX_2 (M=Ca, Cr, Mn, Ni, Cu, Zn) upon MX_2 ··L complex formation [1,2] prompted increased interest in such complexes. Subsequently, similar effect has been detected in the low temperature Ar matrix infrared spectra of the species formed by SnX_2 and PbX_2 halides (X=F, Cl, Br, I) with carbon monoxide, dinitrogen and nitrogen monoxide [3]. Analysis of their infrared spectra led to the conclusion that the structure of SnX_2 ··L and PbX_2 ··L complexes consists of a bent MX_2 moiety with end-on coordinated ligand molecule and the blue shift of intra-ligand stretching mode can be explained in terms of electron density transfer from anti-bonding σ^* orbitals of the ligand to empty d orbitals of the metal [3]. Ab initio study of PbX_2 ··L compounds (L=CO, N_2; X=F, Cl, Br, I) at MP2 level with relativistic effective core potentials (RECP) and basis sets of SBKJC+(d) type afforded description of equilibrium geometry of these species and correctly reproduced, at anharmonic level, shift of ν(N≡N) and ν(C=O) stretching modes to higher energy upon complex formation [4]. Electronic structure of nitrogen monoxide [5] and its complexes with transition metals [6,7] have been extensively studied both experimentally and by computational chemistry methods. Interaction of NO with silver [8], gold [9], and platinum [10] small metal clusters as well as with transition metal clusters embedded in zeolites [11] has also been a subject of considerable interest with relation to heterogeneous catalysis. Variety of binding modes of the NO molecule to metal atoms, resulting in linear N-coordinated, linear O-coordinated, bent N- or O-coordinated, and side-on η^2 coordinated structures have been either observed experimentally [6-11] or investigated by quantum chemistry methods [6,12]. Amongst the computational chemistry methods employed to the elucidation of electronic structure and properties of open-shell systems like nitrogen monoxide complexes with metals and metal ions, perturbational treatment of electron

correlation based on restricted open-shell Hartree-Fock (ROHF) reference wave function has been preferred to unrestricted Möller-Plesset (MP) perturbation theory because of better convergence properties and lesser sensitivity to spin contamination [13-17]. Characteristics of Z-averaged perturbation theory (ZAPT) [13,14], based on ROHF reference wave function, appear particularly interesting as the computational demand of the method is comparable to that of the closed-shell MP method [14] and it is entirely devoid of spin contamination at second order (ZAPT2) [14]. Moreover, since the analytic gradient expressions for second order ZAPT theory have been derived [15] and implemented in revised form within distributed data interface [16], thus enabling parallel execution of the code on computer clusters, the method seems even more attractive for treatment of large open-shell molecular systems and detailed PES scans on such molecules. Binding mode of the NO molecule and geometry of the complexes have been commonly inferred from the infrared spectra of species trapped in low temperature rare gas matrices [3,6] aided with density functional theory (DFT) calculations of the harmonic approximation vibrational spectra [6]. Properties of metal cluster bound NO have been studied by DFT method [8,10,12] or first-principles based simulation packages like VASP [9,11]. In most cases, vibrational spectra computed in the harmonic approximation have been used to establish NO binding mode and provide support to experimental transition assignments, except for the most recent VASP study on nitric oxide adsorption on Pd clusters in mordenite [11], where one-dimensional treatment of NO anharmonicity has been applied. The importance of anharmonic treatment of nitric oxide complexes becomes evident from the analysis of the latter data [11], where the red shift of ν(N=O) stretching mode of Pd cluster bound NO is contrasted with the blue shift of this mode in mordenite supported Pd clusters.

Vibrational self-consistent field (VSCF) theory [18-22], an analog of self-consistent field method in electronic structure theory, provides a route to computation of anharmonic

approximation vibrational spectrum by taking into account intrinsic anharmonicity related to vibrational motion along single normal mode in the mean field of the remaining modes, as well as that originating in inter-mode coupling. PES points required by the direct VSCF method are computed on a rectangular grid derived from normal mode displacements in rectilinear [23,24] or curvilinear (internal) [25] coordinates along single modes and mode pairs (and possibly mode triples) by electronic structure method of choice. It has been shown that VSCF method based on PES grid derived from normal mode displacements in curvilinear coordinates provides better description of low energy large amplitude vibrations [25] as compared to that employing grid deduced from rectilinear coordinates [23,24]. Correlation corrected extensions of VSCF method, termed CC-VSCF, based on either virtual configuration interaction (VCI) including singly and doubly excited states [23,26] or second-order non-degenerate [23,26] and degenerate [27,28] perturbation theory account for inter-mode correlation effects. CC-VSCF method has been successfully applied to weakly bound species like rare gas (Rg) hydrogen fluoride HRgF complexes [29], HXeI [30], HXeOH [31], as well as to $PbX_2 \cdot\cdot L$ complexes (X= F, Cl, Br, I; L= CO, N_2) [4]. Noticeably, VSCF method provided correct explanation of the anomalous isotope effect in the spectrum of HXeOH [31], and a blue shift of ν(N≡N) and ν(C=O) stretching modes upon $PbX_2 \cdot\cdot L$ complex formation [4]. Having this in mind, one can anticipate that anharmonic level description of open-shell $PbX_2 \cdot\cdot NO$ and $PbX_2 \cdot\cdot ON$ species (X=F, Cl, Br, I) vibrational spectra by correlation corrected VSCF method seems feasible.

Present work reports on ZAPT2/SBKJC+(d) level computation of equilibrium geometry parameters and CC-VSCF anharmonic vibrational spectra of $PbX_2 \cdot\cdot NO$ and $PbX_2 \cdot\cdot ON$ bonding isomers (X=F, Cl, Br, I). Anharmonic wavenumber shifts of ν(N=O), ν_s(Pb-X), and ν_{as}(Pb-X) fundamentals upon $PbX_2 \cdot\cdot NO$ complex formation are compared to those observed in the low temperature Ar matrix spectra [3] and correspondingly to those of $PbX_2 \cdot\cdot ON$

isomer species. Influence of mode-mode coupling strength on anharmonic corrections is also discussed.

2. METHODS

All computations of equilibrium geometry, harmonic approximation vibrational spectra, CC-VSCF fundamentals and overtone transitions were done within electronic structure suite of programs GAMESS [32]. Equilibrium geometry parameters of PbX_2 ··NO and PbX_2··ON (X=F, Cl, Br, I) complexes were evaluated under C_s symmetry constraints using parallel implementation [16] of second-order Z-averaged perturbation theory (ZAPT2) [13-15] and Stevens-Basch-Krauss-Jasien-Cundari (SBKJC) scalar-relativistic effective core potentials (RECP) and valence basis sets on all atoms [33-36]. Replacement of all-electron basis sets by effective core potentials does not lead to significant loss of accuracy even in case of 2-nd and 3-rd row elements [37]. SBKJC basis set was augmented with single d-type polarization and single L-type diffuse functions, denoted as SBKJC+(d). Harmonic approximation vibrational spectra of the complexes were computed from Hessians evaluated by numerical differentiation of analytic ZAPT2 gradients. Two-mode representation of the VSCF system potential [23,26,27], including single mode (diagonal) $V_i^{diag}(Q_i)$ and mode-mode coupling $V_{ij}^{coup}(Q_i, Q_j)$ terms was assumed, based on adequate description of PbX_2··L anharmonicity [4] by such truncated expression:

$$V(Q_1,...Q_N) = \sum_{j}^{N} V_j^{diag}(Q_j) + \sum_{i}^{N-1}\sum_{j>i}^{N} V_{ij}^{coup}(Q_i,Q_j)$$

where N is the number of normal modes and Q_i and Q_j are i-th and j-th normal coordinates. Potential energy and dipole moment surfaces were computed at ZAPT2/SBKJC+(d) level on 16 point grid (diagonal potentials) and 16x16 point square grid (coupling potentials) derived from normal mode displacements in curvilinear (internal) coordinates within $[-4\omega_i^{-0.5}, +4\omega_i^{-}$

$^{0.5}$] range (where ω_i is the frequency of i-th normal mode). Direct CC-VSCF method required calculation of 9360 PES points for each species. Intensities of fundamental transitions were evaluated using ZAPT2 dipole moment surfaces and VSCF wavefunctions of the corresponding states,

$$I_i = \frac{8\pi^3 N_a}{3hc}\omega_i \left| \left\langle \Psi_i^{(0)}(Q_i) \left| \vec{\mu}(Q_i) \right| \Psi_i^{(m)}(Q_i) \right\rangle \right|^2$$

where $\psi_i^{(0)}$ and $\psi_i^{(m)}$ denote VSCF wavefunctions of the ground and the m-th excited vibrational states of i-th normal mode, ω_i is the CC-VSCF vibrational frequency of this mode, and the remaining symbols have their regular meaning [26].

3. RESULTS AND DISCUSSION

3.1. Equilibrium geometry

It seems worth noting that equilibrium bond length of free NO computed at ZAPT2/SBKJC+(d) level (Table 1) is longer than experimental bond distance of 115.1 pm [38] by 4.1 pm, and longer by 3.4 pm with relation to that calculated by ZAPT2 method using triple-zeta quality basis set TZ2P [14]. Although overestimation of r(N=O) distance appears significant, it seems of secondary importance in computation aimed at anharmonic level description of vibrational transitions in PbX_2··NO and PbX_2··ON complexes, including blue shift of ν(N=O) stretching mode upon complex formation. On the other hand, equilibrium bond distances and angles of lead halides evaluated under C_{2v} symmetry by MP2 method in the same basis set (Table 1) overestimate experimental gas phase geometry parameters derived from electron diffraction [39] to a less significant extent with the exception of PbF_2, where r(Pb-F) distance is longer than experimental r_g value by 1.4 pm (Table 1). Nonetheless,

the difference is almost negligible, even when $r_e < r_g$ relationship is taken into account [39]. A noticeable shortening of r(N=O) distance upon PbX_2··NO complex formation (0.2 – 0.3 pm) occurs in concord with halide dependent lengthening of r(Pb-X) distance, amounting to 1.4 pm (PbF_2··NO) – 2.3 pm (PbI_2··NO) (Table 1). Opposite change or no change in r(N=O) bond length is observed on formation of PbX_2··ON species in accord with less pronounced increase in r(Pb-X) distance (0.7 – 1.0 pm) on going from fluoride to iodide. Equilibrium geometry of PbX_2··NO species (Figure 1), characterized by r(Pb-N) bond distance within 266.6 – 271.7 pm, and (Pb-N-O) angle of 109.2 – 120.7 deg, differs considerably from that of PbX_2··N_2 [4] complex by much shorter Pb-N bond length and less obtuse Pb-L-L angle (where L-L represents ligand molecule). Moreover, computed (Pb-N-O) angle in PbX_2··NO series nears that characteristic of N-coordinated NO molecule with sp^2 hybridized nitrogen atom in transition metal complexes [12]. Isomer complex molecule, PbX_2··ON (Figure 2) shows slightly longer Pb-O bond length (Table 1), varying between 267.8 and 275.8 pm, and more obtuse (Pb-O-N) angle, as compared to PbX_2··NO species. Despite remote similarity, it can be noted that the longest Pb-O bond distances of $Pb_4(OH)_4^{4+}$ (252 pm) [45] and $Pb_6O(OH)_6^{4+}$ (267.7 pm) [46] ions, computed at MP2 level in scalar relativistic ECP basis [45,46], are very close to those of PbX_2··ON series. One can also note that lengthening of r(Pb-L) distance and increase in (Pb-L-L) angle in both PbX_2··NO and PbX_2··ON isomers follows the order of decreasing electronegativity of halogen atoms and, in consequence, decreasing positive charge on Pb atom.

3.2. Anharmonic spectra of PbF_2··NO and PbF_2··ON complexes

Harmonic wavenumber of ν(N=O) mode computed at ZAPT2/SBKJC+(d) level (1890.1 cm^{-1}; Table 2) compares favorably against that computed by the same method in triple-zeta valence basis set, TZ2P (1895.8 cm^{-1}) [14]. VSCF computed fundamental of this mode (1869.1 cm^{-1}),

including intrinsic (diagonal) anharmonicity, appears reasonably close to the transition wavenumber observed in the Ar matrix spectrum of NO (1875.0 cm^{-1}) [3], showing deviation typical of VSCF method for stretching modes [23-27]. Since there is no contribution to anharmonic correction from mean field effect or inter-mode correlation in the case of molecule with single vibrational mode, the aforementioned wavenumber of ν(N=O) fundamental will be used to evaluate anharmonic shift of ν(N=O) mode upon complex formation. VSCF computed anharmonic spectra of PbF_2··NO and PbF_2··ON complexes (Table 2) provide fundamentals corrected for intrinsic (diagonal) anharmonicity, mean field and mode-mode coupling (VSCF), and mode correlation at degenerate second order perturbational (DPT2-VSCF) level. For the reason stated above, ν(N=O) fundamental of the coordinated NO, corrected for intrinsic anharmonicity, will be used to assess wavenumber shift due to complex formation. Fundamentals of PbF_2, computed at MP2/SBKJC+(d) level (Table 2), show negligible deviation from low temperature Ne matrix spectrum [42] whereas those of ν_s(Pb-F) and ν_a(Pb-F) modes in PbF_2··NO complex overestimate transition wavenumbers measured in low temperature Ar matrix [3] by ~10 cm^{-1}, partly due to matrix polarizability effects [39]. It seems interesting to note that the harmonic approximation provides qualitatively incorrect description of ν(N=O) mode shift on PbF_2··NO complex formation (-11.7 cm^{-1}) whereas the wavenumber difference of the respective fundamentals (+15.8 cm^{-1}) nears that deduced from experiment (+16.4 cm^{-1}) [3]. Although wavenumber shifts of ν_s(Pb-F) and ν_a(Pb-F) fundamentals on going from PbF_2 to PbF_2··NO are lower than those estimated in the harmonic approximation, they are still larger than shifts assessed experimentally [3]. Wavenumber of high intensity ν(Pb-N) fundamental at 232.8 cm^{-1} is 10 cm^{-1} lower than its harmonic counterpart, with majority of anharmonic correction coming from intrinsic anharmonicity and mean field / mode coupling effects. Same pattern of anharmonic corrections can be observed for all PbF_2··NO fundamentals (Table 2), whereas

contribution to anharmonicity resulting from mode correlation appears significant only in the case of ν_a(Pb-F) mode, leading to 0.8 cm^{-1} difference between VSCF and DPT2-VSCF wavenumbers. Analysis of the mode-mode coupling pattern of PbF_2··NO vibrational modes, represented as a two-dimensional mapping of $V_{i,j}^{coup}(Q_i, Q_j)$ mode coupling potential (Figure 3) on NxN PES grid,

$$P(Q_i, Q_j) = \begin{Bmatrix} N\sum_{p=1}^{N} |V(n_{ip})| \; if \; i = j \\ \sum_{p=1}^{N}\sum_{q=1}^{N} |V(n_{ip}, n_{jq})| \; otherwise \end{Bmatrix}$$

where n_{ip} and n_{jq} are grid points and N is the number of grid points (N=16), reveals that inter-mode coupling contribution to VSCF anharmonic correction seems substantial for ν_s(Pb-F) and ν_a(Pb-F), ν(Pb-N) and $\rho_w(PbF_2)$, $\rho_w(PbF_2)$ and $\rho_t(PbF_2)$ mode pairs. Since no experimental evidence of PbX_2··ON complexes has been reported to date, their anharmonic spectra can be compared against those of PbX_2··NO isomer or structurally similar lead(II) compounds. Fundamental transitions of PbF_2··ON isomer (Table 2) can be viewed as characteristics of O-coordinated NO molecule, as evidenced by 33.4 cm^{-1} red shift of ν(N=O) stretching mode upon complex formation and less pronounced shifts of ν_s(Pb-F) and ν_a(Pb-F) fundamentals on going from PbF_2 to PbF_2··ON. Wavenumber of ν(Pb-O) fundamental, computed at 183.2 cm^{-1}, shows significant anharmonic correction due to intrinsic anharmonicity and mean field / mode coupling and appears remarkably close to the lowest energy ν(Pb-O) stretching mode of $Pb_6O(OH)_6^{4+}$ ion (179 cm^{-1}) [46], evaluated in the harmonic approximation at MP2/ECP level. Anharmonic corrections of PbF_2··ON modes lack significant contribution from mode correlation with the exception of $\rho_t(PbF_2)$ twisting mode, where DPT2-VSCF fundamental appears 2.8 cm^{-1} above its VSCF analog. Mapping of PbF_2··ON coupling potentials (Figure 4), evaluated at ZAPT2/SBKJC+(d) level, indicates that ν_s(Pb-F) and ν_a(Pb-F), ν(Pb-O) and $\rho_w(PbF_2)$, $\rho_w(PbF_2)$ and $\rho_t(PbF_2)$ mode pairs are strongly

coupled, which leads in consequence to sizable VSCF anharmonic corrections of the respective fundamentals. Similarity of mode coupling patterns of PbF_2··NO and PbF_2··ON implies that interaction between mode pairs does not depend substantially on NO coordination mode, but rather involves fundamentals originating in analogous normal mode displacements, like $\rho_w(PbF_2)$ and $\rho_t(PbF_2)$ mode pair of both isomers. Same characteristics of the two-dimensional mapping of mode coupling potential pertain to the remaining members of PbX_2··NO and PbX_2··ON series, so that their coupling patterns are not reported here for the sake of brevity. VSCF computation predicts the most intense overtone and combination transitions of PbF_2··NO and PbF_2··ON complexes (Table 2a) to originate in ν_s(Pb-F), ν_a(Pb-F), ν(Pb-N), ν(Pb-O), $\rho_w(PbF_2)$, and τ(N=O) modes, which display high intensity fundamentals and are mutually coupled to an appreciable extent (Figures 2 and 3). Anharmonic corrections of overtones and combination transitions (Table 2a) almost exclusively stem from diagonal anharmonicity and mean field / coupling effects whereas contribution of inter-mode correlation appears nearly negligible.

3.3. Anharmonic spectra of $PbCl_2$··NO and $PbCl_2$··ON complexes

Fundamentals of $PbCl_2$, computed at MP2/SBKJC+(d) level, are reported in Table 3 as a reference enabling evaluation of wavenumber shift of ν_s(Pb-Cl) and ν_a(Pb-Cl) modes resulting from complex formation. Their wavenumbers overestimate experimental Ar matrix spectrum [3] by 12 – 29.7 cm^{-1} due to matrix polarizability effects as well as inaccuracy of the VSCF method itself. Vibrational transitions of $PbCl_2$··NO and $PbCl_2$··ON isomers (Table 3) are weakly anharmonic with the exception of ν(Pb-N), ν(Pb-O), $\rho_w(PbCl_2)$, $\rho_t(PbCl_2)$, and τ(N=O) modes, whose DPT2-VSCF fundamentals are 4 – 10 cm^{-1} lower in energy than their harmonic equivalents. Anharmonic corrections of $PbCl_2$··NO and $PbCl_2$··ON modes originate

for the most part in diagonal anharmonicity and mean field / coupling effects with minor contribution from mode-mode correlation. Wavenumber shift of ν(N=O) fundamental on $PbCl_2$··NO complex formation is smaller than that calculated for PbF_2··NO species and amounts to 14.2 cm^{-1}, in accord with reduced σ donation from NO molecule to less positively charged lead ion [3]. Similar effect can be observed in the VSCF spectrum of $PbCl_2$··ON complex, where O-coordination of NO molecule generates oppositely signed shift of ν(N=O) fundamental by -30.7 cm^{-1} as compared to -33.4 cm^{-1} in PbF_2··ON (Table 6). For the same reason the change in energy of ν_s(Pb-Cl) and ν_a(Pb-Cl) fundamentals on going from $PbCl_2$ to $PbCl_2$··NO, amounting to -8.9 cm^{-1} and -8.6 cm^{-1}, respectively, is much smaller than that computed for the fluoride analog. The same effect is also responsible for the decreased wavenumber shifts of ν_s(Pb-Cl) and ν_a(Pb-Cl) fundamentals upon $PbCl_2$··ON complex formation. Discernible diminution of the wavenumbers of ν(Pb-N) and ν(Pb-O) fundamentals in $PbCl_2$··NO and $PbCl_2$··ON complexes with relation to fluoride analogs (Table 3) can be attributed to the weakening of Pb-N and Pb-O bonds on fluoride to chloride substitution caused by diminished σ donation from NO molecule, mentioned above. Anharmonic corrections of τ(N=O) torsional mode in $PbCl_2$··NO and $PbCl_2$··ON isomers stem for the most part from mean field / mode coupling effects and appear coordination mode dependent, leading to 18.6 cm^{-1} difference between harmonic and VSCF wavenumber of this mode in the case of O-coordinated NO molecule.

3.4. Anharmonic spectra of $PbBr_2$··NO and $PbBr_2$··ON complexes

The assignment of ν_s(Pb-Br) and ν_a(Pb-Br) streching modes in the gas phase spectrum of $PbBr_2$, placing antisymmetric mode at higher energy than symmetric one [43] contradicts the order observed in other PbX_2 halides [3] and also that of VSCF computed fundamentals [4]

(Table 4). Therefore, a reversal of experimental assignment placing ν_s(Pb-Br) mode higher in energy than ν_a(Pb-Br) would be consistent with VSCF calculation and VSCF computed intensity pattern of these two fundamentals (Table 4). Fundamentals of $PbBr_2$··NO and $PbBr_2$··ON isomers are weakly anharmonic with no significant contribution to anharmonicity from correlation correction. Fundamental of ν(N=O) mode shows blue shift of 14.6 cm^{-1} on $PbBr_2$··NO complex formation whereas creation of O-coordinated $PbBr_2$··ON species results in -28.0 cm^{-1} red shift of this mode. It can also be noted (Table 4) that significant coupling of ν(Pb-N) mode of $PbBr_2$··NO to ν_s(Pb-Br) symmetric stretch results in sizable increase of ν_s(Pb-Br) fundamental intensity, making it almost indistinguishable from that of ν_a(Pb-Br) antisymmetric stretching fundamental. Wavenumbers of ν_s(Pb-Br) and ν_a(Pb-Br) fundamentals in $PbBr_2$··NO are lower than those of the analogous modes in $PbBr_2$ by -3.0 and -6.3 cm^{-1}, respectively, while formation of $PbBr_2$··ON complex shifts both modes to lower energy by -3.1 cm^{-1}. A decrease in the energy of ν(Pb-N) and ν(Pb-O) fundamentals in $PbBr_2$··NO and $PbBr_2$··ON isomers with relation to those of the fluoride and chloride analogs follows the order of decreasing positive charge on lead(II) ion and, in consequence, decreasing Pb-N and Pb-O bond strengths. Interestingly, sensitivity of the vibrational modes involving $PbBr_2$ moiety as a whole, $\rho_w(PbBr_2)$ and $\rho_t(PbBr_2)$, to the NO coordination mode can be viewed as a demonstration of difference in Pb-N and Pb-O bond strengths.

3.5. Anharmonic spectrum of PbI_2··ON complex

Fundamental transitions of PbI_2 computed by DPT2-VSCF method (Table 5) are weakly anharmonic and their wavenumbers do not differ appreciably from Ar and Kr matrix spectra extrapolated to zero matrix polarizability [39]. Since the VSCF procedure did not converge in the case of PbI_2··NO complex, only anharmonic spectrum of PbI_2··ON species is reported in

Table 5. The red shift of ν(N=O) fundamental on PbI_2··ON complex formation (-30.4 cm^{-1}) exceeds that calculated in the harmonic approximation (-25.5 cm^{-1}), revealing the importance of anharmonic correction in the case of ν(N=O) mode. The wavenumber of ν(Pb-O) fundamental (150.7 cm^{-1}) differs from its harmonic counterpart by 8.6 cm^{-1} due to nearly equal diagonal and mean field / mode coupling contributions to anharmonic correction. The energy of that mode is the lowest in PbX_2··ON series, in agreement with the trend observed for other members of the series. VSCF computed shifts of ν_s(Pb-I) and ν_a(Pb-I) fundamentals upon complex formation, -1.4 and -2.1 cm^{-1}, respectively, are significantly lower than those evaluated for the other PbX_2··ON species, due to dramatically weakened σ-donation from the ligand. In line with the characteristics of PbF_2··ON and $PbCl_2$··ON anharmonic spectra, the lowest energy τ(N=O) torsional mode fundamental shows exceptionally large anharmonic correction, stemming mostly from intrinsic anharmonicity with smaller contributions arising from VSCF and mode correlation effects.

4. CONCLUSIONS

Equilibrium geometry parameters of the open-shell PbX_2··NO and PbX_2··ON species, evaluated at ZAPT2/SBKJC+(d) level, depict both isomers as NO molecule end-on coordinated to PbX_2 halide with NO molecular axis nearly parallel to the PbX_2 plane (Figures 1 and 2). Computation of the anharmonic approximation vibrational spectra of PbX_2··NO (X=F, Cl, Br) and PbX_2··ON (X=F, Cl, Br, I) complexes by DPT2-VSCF method at the same level of theory afforded satisfactory description of the experimental Ar matrix spectrum of PbF_2··NO species [3] and provided sensibly consistent predictions of the spectra of the remaining compounds. Harmonic approximation based wavenumber shift of the ν(N=O) mode upon PbX_2··NO complex formation (Table 6) appears qualitatively incorrect as being oppositely signed to the experimental one, whereas that computed from VSCF fundamentals

agrees with experiment within a fraction of a wavenumber (PbF_2··NO). VSCF computed wavenumbers of ν(Pb-N) and ν(Pb-O) stretching mode fundamentals of the respective bonding isomers decrease in accord with the decreasing ionic character of Pb-X bond, following the order: F > Cl > Br > I. Energy changes of ν_s(Pb-X) and ν_a(Pb-X) fundamentals on going from PbX_2 to PbX_2··NO and PbX_2··ON species conform to the same trend (Table 6), with VSCF computed values being closer to the experiment. Despite substantial overestimation of r(N=O) bond length at ZAPT2/SBKJC+(d) level, the fundamental of ν(N=O) mode, corrected for intrinsic anharmonicity, provided satisfactory description of coordination mode dependent changes in ν(N=O) mode wavenumber upon complex formation.

ACKNOWLEDGEMENTS

A generous grant of the computer time from the Wrocław Center for Networking and Supercomputing (WCSS) is gratefully acknowledged.

References

1. D.A. Van Leirsburg, C. W. DeKock, J. Am. Chem. Soc. **94**, 3235 (1972)
2. D.A. Van Leirsburg, C. W. DeKock, J. Phys. Chem. **78**, 134 (1974)
3. D. Tevault, K. Nakamoto, Inorg. Chem. **15**, 1282 (1975)
4. A. T. Kowal, J. Mol. Struct. (Theochem) **761**, 119 (2006)
5. Ch. A. Arrington, T. H. Dunning, Jr., D. E. Woon, J. Phys. Chem. A **111**, 11185 (2007)
6. L. Andrews, A. Citra, Chem. Rev. **102**, 885 (2002)
7. P. Hummel, J. R. Winkler, H. B. Gray, Theor. Chem. Account **119**, 35 (2008)
8. J. Zhou, F. Xiao, W-N. Wang, K-N. Fan, J. Mol. Struct. (Theochem) **818**, 51 (2007)
9. W. Zhang, Z. Li, Y. Luo, J. Yang, J. Chem. Phys. **129**, 134708 (2008)
10. N. U. Zhanpeisov, H. Fukumura, J. Chem. Theory. Comput. **2**, 801 (2006)
11. R. Grybos, L. Benco, T. Bučko, J. Hafner, J. Chem. Phys. **130**, 104503 (2009)
12. K. R. Sawyer, R. P. Steele, E. A. Glascoe, J. F. Cahoon, J. P. Schlegel, M. Head-Gordon, Ch. B. Harris, J. Phys. Chem. A **112**, 8505 (2008)
13. T. J. Lee, D. Jayatilaka, Chem. Phys. Lett. **201**, 1 (1993)
14. T. J. Lee, A. P. Rendell, K. G. Dyall, D. Jayatilaka, J. Chem. Phys. **100**, 7400 (1994)
15. G. D. Fletcher, M. S. Gordon, R. S. Bell, Theor. Chem. Acc. **107**, 57 (2002)
16. C. M. Aikens, G. D. Fletcher, M. W. Schmidt, M. S. Gordon, J. Chem. Phys. **124**, 014107 (2006)
17. S. E. Wheeler, W. D. Allen, H. F. Schaefer III, J. Chem. Phys. **128**, 074107 (2008)
18. J. M. Bowman, J. Chem. Phys. **69**, 608 (1978)
19. R. B. Gerber, M. A. Ratner, Chem. Phys. Lett. **68**, 195 (1979)
20. H. Romanowski, J. M. Bowman, L. B. Harding, J. Chem. Phys. **82**, 4155 (1985)
21. J. M. Bowman, Acc. Chem. Res. **19**, 202 (1986)

22. R. B. Gerber, M. A. Ratner, Adv. Chem. Phys. **70**, 97 (1988)

23. J.O. Jung, R.B. Gerber, J. Chem. Phys. **105**, 10332 (1996)

24. Y. Miller, G. M. Chaban, and R. B. Gerber, Chem. Phys. **313**, 213 (2005)

25. B. Njegic, M. S. Gordon, J. Chem. Phys. **125** (2006) 224102

26. G.M. Chaban, J.O. Jung, R.B. Gerber, J. Chem. Phys. **111**, 1823 (1999)

27. N. Matsunaga, G.M. Chaban, R.B. Gerber, J. Chem. Phys. **117**, 3541 (2002)

28. K. Yagi, S. Hirata, K. Hirao, Phys. Chem. Chem. Phys. **10**, 1781 (2008)

29. J. Lundell, G. M. Chaban, R. B. Gerber, Chem. Phys. Lett. **331**, 308 (2000)

30. J. Lundell, M. Pettersson, L. Khriachtchev, M. Räsänen, G. M. Chaban, R. B. Gerber, Chem. Phys. Lett. **322**, 389 (2000)

31. L. Khriachtchev, J. Lundell, M. Pettersson, H. Tanskanen, M. Räsänen, J. Chem. Phys. **116**, 4758 (2002)

32. M. W. Schmidt, K. K. Baldridge, J. A. Boatz, S. T. Elbert, M. S. Gordon, J. J. Jensen, S. Koseki, N. Matsunaga, K. A. Nguyen, S. Su, T. L. Windus, M. Dupuis, J. A. Montgomery, J. Comput. Chem. **14**, 1347 (1993)

33. W. J. Stevens, H. Basch, M. Krauss, J. Chem. Phys. **81**, 6026 (1984)

34. W. J. Stevens, M. Krauss, H. Basch, P. G. Jasien, Can. J. Chem. **70**, 612 (1992)

35. T. R. Cundari, W. J. Stevens, J. Chem. Phys. **98**, 5555 (1993)

36. B. M. Bode, M. S. Gordon, J. Chem. Phys. **111**, 8778 (1999)

37. D. M. Benoit, J. Chem. Phys. **120**, 562 (2004)

38. K. P. Huber, G. Herzberg, "Molecular Spectra and Molecular Structure. IV. Constants of Diatomic Molecules", Van Nostrand Reinhold, New York 1979

39. M. Hargittai, Chem. Rev. **2000,** 2233 (2000)

40. M. Benavides-Garcia, K. Balasubramanian, J. Chem. Phys. **100**, 2821 (1994)

41. S. Escalante, R. Vargas, A. Vela, J. Phys. Chem. A **103**, 5590 (1999)

42. R. H. Hauge, J. W. Hastie, J. L. Margrave, J. Mol. Spectrosc. **45**, 420 (1973)

43. L. Brewer, G. R. Somayajulu, E. Brackett, Chem. Rev. **63**, 111 (1963)

44. G. Schaftenaar, J. H. Noordik, J. Comput.-Aided Mol. Design **14**, 123 (2000)

45. J. O. Jensen, J. Mol. Struct. (Theochem) **587**, 111 (2002)

46. J. O. Jensen, J. Mol. Struct. (Theochem) **635**, 11 (2002)

Figure captions

Figure 1. Equilibrium geometry of PbX_2··NO complexes computed at ZAPT2/SBKJC+(d) level (Molden [44] drawing).

Figure 2. Equilibrium geometry of PbX_2··ON complexes computed at ZAPT2/SBKJC+(d) level (Molden [44] drawing).

Figure 3. Two-dimensional mapping of $V_{i,j}^{coup}(Q_i , Q_j)$ mode coupling potential of PbF_2··NO at ZAPT2/SBKJC+(d) level. Modes are labeled in the order of decreasing harmonic wave number (first column of Table 2) and the relative strength of the potential is coded in shades of gray (0, white and 255, black).

Figure 4. Two-dimensional mapping of $V_{i,j}^{coup}(Q_i , Q_j)$ mode coupling potential of PbF_2··ON at ZAPT2/SBKJC+(d) level. Modes are labeled in the order of decreasing harmonic wave number (first column of Table 2) and the relative strength of the potential is coded in shades of gray (0, white and 255, black).

Table 1. Structural parameters of PbX_2 halides and PbX_2··L (X=F, Cl, Br, I; L=NO) complexes computed at MP2/SBKJC+(d) and ZAPT2/SBKJC+(d) level, respectively.

Compound	r(Pb-X) [pm]		<(X-Pb-X) [°]		r(Pb-L) [pm]	<(Pb-L) [°]	r(L-L)[e] [pm]
	Calcd.	Exptl.	Calcd.	Exptl.	Calcd.	Calcd.	Calcd.
NO							119.2
PbF_2	205.0	203.6[a]	98.0	97.8[c], 98.5[a]			
PbF_2··NO	206.4		97.3		266.6	109.2	119.0
PbF_2··ON	205.7		98.1		267.8	117.1	119.3
$PbCl_2$	244.1	244.5[a]	98.3	96±3[d], 100.8			
$PbCl_2$··NO	245.7		98.6		269.1	115.5	119.0
$PbCl_2$··ON	244.8		98.8		270.7	124.5	119.2
$PbBr_2$	258.6	257.9[b]	99.5	98.8[d]			
$PbBr_2$··NO	260.6		99.9		270.7	117.8	118.9
$PbBr_2$··ON	259.5		100.1		273.5	125.5	119.2
PbI_2	279.9	280.7[a]	100.6	99.7[d]			
PbI_2··NO	282.1		101.1		271.7	120.7	118.9
PbI_2··ON	280.9		101.1		275.8	127.8	119.2

[a]- r_g Ref. [39] [b] – r_e Ref. [39]

[c] – Ref. [41] [d] – Ref. [40]

[e] - r_e(NO)=115.1 pm Ref. [38]

Table 2. Vibrational transitions (cm^{-1}) of PbF_2, and PbF_2··NO, PbF_2··ON complexes calculated at MP2/SBKJC+(d), ZAPT2/SBKJC+(d) level by direct VSCF method.

	Mode	Harmonic	Diagonal	VSCF	DPT2-VSCF	Intensity [km/mole]	Exptl.[a]	Assignment[c]
PbF_2	1	550.7	549.0	548.1	546.7	88.8	545.7[b] 531.4	ν_s(Pb-F)
	2	527.5	529.4	524.2	523.5	132.0	522.5[b] 507.2	ν_a(Pb-F)
	3	163.7	163.8	162.6	162.6	14.1	170[b]	δ(F-Pb-F)
NO	1	1890.1	1869.1			12.4	1875.0	ν(N-O)
PbF_2··NO	1	1878.4	1884.9	1879.8	1879.8	3.0	1891.4	ν(N-O)
	2	535.1	533.4	533.1	532.7	79.2	522.6	ν_s(Pb-F)
	3	513.0	515.1	510.3	509.5	127.2	498.7	ν_a(Pb-F)
	4	243.6	238.6	232.8	232.8	109.7		ν(Pb-N)
	5	168.3	168.2	166.8	166.8	16.4		δ(F-Pb-F)
	6	128.2	127.2	123.4	123.7	1.2		$\rho_w(PbF_2)$ ip
	7	97.8	96.8	94.5	94.2	44.7		$\rho_w(PbF_2)$ op
	8	92.1	93.7	87.1	87.2	0.9		$\rho_t(PbF_2)$
	9	68.2	66.5	60.0	59.9	119.7		τ(N-O)
PbF_2··ON	1	1861.6	1835.7	1836.5	1836.4	28.6		ν(N-O)
	2	542.6	540.9	540.7	540.3	81.1		ν_s(Pb-F)
	3	519.9	521.9	517.3	516.5	130.0		ν_a(Pb-F)
	4	196.3	190.6	183.1	183.2	91.0		ν(Pb–O)
	5	165.1	165.0	163.9	163.9	13.9		δ(F-Pb-F)
	6	105.0	103.6	98.4	98.8	0.9		$\rho_w(PbF_2)$ ip
	7	79.1	78.2	76.2	75.8	51.6		$\rho_w(PbF_2)$ op
	8	75.9	70.6	61.3	58.4	123.0		τ(N-O)
	9	74.9	76.4	69.8	72.6	15.3		$\rho_t(PbF_2)$

[a] – Ar matrix data Ref. [3]

[b] – Ne matrix data Ref. [42]

[c] – ν- stretching, δ - deformation, ρ_r – rocking, ρ_w – wagging, ρ_t – twisting, τ – torsional, ip – in-phase mode, op – out-of-phase mode

Table 2a. Most intense (I > 1.0 km/mole) overtone and combination transitions (cm^{-1}) of PbF_2, and PbF_2··NO, PbF_2··ON complexes calculated at MP2/SBKJC+(d), ZAPT2/SBKJC+(d) level by direct VSCF method.

	Harmonic	Diagonal	VSCF	DPT2-VSCF	Intensity [km/mole]	Assignment[a]
PbF_2	1078.2	1078.4	1071.8	1069.9	1.2	ν_s(Pb-F) + ν_a(Pb-F)
PbF_2··NO	1048.2	1048.5	1042.6	1040.8	1.2	ν_s(Pb-F) + ν_a(Pb-F)
	603.3	599.9	593.3	592.9	2.9	ν_s(Pb-F) + τ(N-O)
	581.2	581.5	570.5	569.7	4.7	ν_a(Pb-F) + τ(N-O)
	487.2	471.9	458.1	458.1	1.6	2 ν(Pb-N)
	371.8	365.8	353.5	353.5	2.8	ν(Pb-N) + $\rho_w(PbF_2)$ ip
	341.4	335.4	325.2	325.2	1.1	ν(Pb-N) + $\rho_w(PbF_2)$ op
	311.8	305.1	291.3	291.3	1.2	ν(Pb-N) + τ(N-O)
	196.4	193.6	181.9	181.9	4.6	$\rho_w(PbF_2)$ ip + τ(N-O)
	136.3	131.8	117.8	117.7	3.3	2 τ(N-O)
PbF_2··ON	1062.5	1062.8	1057.3	1055.4	1.2	ν_s(Pb-F) + ν_a(Pb-F)
	618.4	611.5	602.4	602.0	2.8	ν_a(Pb-F) + τ(N-O)
	595.8	592.5	579.0	578.3	5.3	ν_a(Pb-F) + τ(N-O)
	392.6	374.9	357.5	357.5	2.5	2 ν(Pb–O)
	301.4	294.2	276.7	276.6	2.3	ν(Pb–O) + $\rho_w(PbF_2)$ ip
	275.5	268.9	257.0	257.0	1.6	ν(Pb-O) + $\rho_w(PbF_2)$ op
	180.9	174.2	156.9	156.9	4.1	$\rho_w(PbF_2)$ ip + τ(N-O)
	158.3	155.5	150.7	150.7	1.3	2 $\rho_w(PbF_2)$ op
	155.0	148.8	136.8	136.8	6.0	$\rho_w(PbF_2)$ op + τ(N-O)
	151.7	137.0	116.8	116.8	3.3	2 τ(N-O)
	150.8	147.0	126.4	126.4	1.2	τ(N-O) + $\rho_t(PbF_2)$

[a] – ν - stretching, δ - deformation, ρ_w – wagging, ρ_t – twisting, τ – torsional, ip – in-phase mode, op – out-of-phase mode

Table 3. Vibrational transitions (cm^{-1}) of $PbCl_2$ and $PbCl_2$··NO, $PbCl_2$··ON complexes calculated at MP2/SBKJC+(d), ZAPT2/SBKJC+(d) level by direct VSCF method.

	Mode	Harmonic	Diagonal	VSCF	DPT2-VSCF	Intensity [km/mole]	Exptl[a]	Assignment[c]
$PbCl_2$	1	349.1	348.2	347.9	347.9	50.5	321.6	ν_s(Pb-Cl)
	2	331.1	332.1	329.6	329.6	106.6	299.9	ν_a(Pb-Cl)
	3	111.5	111.5	111.0	111.0	3.9	99[b]	δ(Cl-Pb-Cl)
NO	1	1890.1	1869.1			12.4	1875.0	ν(N-O)
$PbCl_2$··NO	1	1886.0	1883.3	1881.9	1881.9	4.1		ν(N-O)
	2	340.0	339.2	339.0	339.0	47.6		ν_s(Pb-Cl)
	3	322.3	323.3	321.0	321.0	99.0		ν_a(Pb-Cl)
	4	228.3	223.9	219.5	219.5	106.6		ν(Pb-N)
	5	122.1	121.8	118.2	118.3	0.9		$\rho_w(PbCl_2)$ ip
	6	107.3	107.2	106.1	106.1	10.5		δ(Cl-Pb-Cl)
	7	79.4	80.1	76.2	76.8	7.2		$\rho_t(PbCl_2)$
	8	76.6	76.2	74.2	74.1	21.2		$\rho_w(PbCl_2)$ op
	9	36.7	40.5	34.9	34.1	128.3		τ(N-O)
$PbCl_2$··ON	1	1864.3	1838.4	1838.7	1838.7	25.6		ν(N-O)
	2	344.9	344.1	344.0	344.0	46.3		ν_s(Pb-Cl)
	3	327.3	328.3	326.1	326.1	102.5		ν_a(Pb-Cl)
	4	180.6	174.9	170.4	170.4	79.9		ν(Pb-O)
	5	111.6	111.7	111.0	111.0	3.4		δ(Cl-Pb-Cl)
	6	93.9	92.4	88.6	88.8	10.9		$\rho_w(PbCl_2)$ ip
	7	67.0	68.0	63.4	63.5	8.5		$\rho_t(PbCl_2)$
	8	63.2	62.8	61.8	61.5	27.1		$\rho_w(PbCl_2)$ op
	9	53.9	41.8	35.3	35.2	138.6		τ(N-O)

[a] – Ar matrix data Ref. [3]

[b] – gas phase data Ref. [43]

[c] – ν - stretching, δ - deformation, ρ_r – rocking, ρ_w – wagging, ρ_t - twisting, τ – torsional, ip – in-phase mode, op – out-of-phase mode

Table 4. Vibrational transitions (cm^{-1}) of $PbBr_2$ $PbBr_2$··NO, $PbBr_2$··ON complexes calculated at MP2/SBKJC+(d), ZAPT2/SBKJC+(d) level by direct VSCF method.

	Mode	Harmonic	Diagonal	VSCF	DPT2-VSCF	Intensity [km/mole]	Exptl.	Assignment[c]
$PbBr_2$	1	232.2	231.8	231.6	231.6	22.6	247[a]	ν_s(Pb-Br)
	2	222.8	223.3	222.1	222.1	60.0	251[a]	ν_a(Pb-Br)
	3	71.7	71.7	71.5	71.5	1.1	59[a]	δ(Br-Pb-Br)
NO	1	1890.1	1869.1			12.4	1875.0[b]	ν(N-O)
$PbBr_2$··NO	1	1888.6	1883.7	1881.4	1881.3	4.7		ν(N-O)
	2	231.2	230.7	228.6	228.6	55.4		ν_s(Pb-Br)+{ (Pb-N)
	3	216.4	216.8	215.8	215.8	55.7		ν_a(Pb-Br)
	4	213.9	213.4	209.0	209.0	65.0		ν(Pb-N)+ν_s(Pb-Br)
	5	114.6	113.4	109.8	109.8	4.8		ρ_w($PbBr_2$) ip
	6	72.7	72.7	71.8	71.8	6.6		δ(Br-Pb-Br)
	7	62.0	62.7	59.8	61.1	5.0		ρ_t($PbBr_2$)
	8	58.1	58.0	56.9	56.8	8.5		ρ_w($PbBr_2$) op
	9	12.9	31.9	26.5	24.9	119.0		τ(N-O)
$PbBr_2$··ON	1	1863.9	1841.1	1840.0	1840.0	25.7		ν(N-O)
	2	229.4	228.9	228.5	228.5	21.3		ν_s(Pb-Br)
	3	219.8	220.3	219.0	219.0	57.6		ν_a(Pb-Br)
	4	170.2	166.9	165.1	165.2	75.6		ν(Pb-O)
	5	90.3	91.0	89.2	89.2	15.4		ρ_w($PbBr_2$) ip
	6	71.1	71.1	70.9	70.9	4.1		δ(Br-Pb-Br)
	7	55.2	57.7	52.8	53.1	77.9		ρ_t($PbBr_2$)
	8	48.5	48.3	47.3	47.3	13.9		ρ_w($PbBr_2$) op
	9	47.8	47.3	47.2	47.1	65.3		τ(N-O)

[a] – gas phase data Ref. [43]

[b] - Ar matrix data Ref. [3]

[c] – ν - stretching, δ - deformation, ρ_r – rocking, ρ_w – wagging, ρ_t - twisting, τ – torsional, ip – in-phase mode, op – out-of-phase mode

Table 5. Vibrational transitions (cm^{-1}) of PbI_2 and PbI_2··ON complex calculated at MP2/SBKJC+(d), ZAPT2/SBKJC+(d) level by direct VSCF method.

	Mode	Harmonic	Diagonal	VSCF	DPT2-VSCF	Intensity [km/mole]	Exptl.	Assignment[c]
PbI_2	1	176.7	176.5	176.3	176.3	13.2	168[a]	ν_s(Pb-I)
	2	171.8	172.1	171.3	171.3	46.0	163[a]	ν_a(Pb-I)
	3	54.3	54.3	54.1	54.1	0.4	43[a]	δ(I-Pb-I)
NO	1	1890.1	1869.1			12.4	1875.0[b]	ν(N-O)
PbI_2··ON	1	1864.6	1838.7	1838.9	1838.9	22.4		ν(N-O)
	2	175.5	175.3	174.8	174.9	17.1		ν_s(Pb-I)
	3	169.4	169.7	169.2	169.2	45.0		ν_a(Pb-I)
	4	159.4	155.7	150.8	150.7	57.0		ν(Pb-O)
	5	85.9	83.4	79.3	79.4	11.8		$\rho_w(PbI_2)$ ip
	6	54.8	54.8	54.6	54.6	2.9		δ(I-Pb-I)
	7	48.6	48.7	43.8	44.8	51.9		$\rho_t(PbI_2)$
	8	42.3	42.3	41.6	41.4	7.9		$\rho_w(PbI_2)$ op
	9	40.5	30.7	25.1	23.9	72.5		τ(N-O)

[a] – Ar and Kr matrix data extrapolated to zero polarizability Ref. [39]

[b] – Ar matrix data Ref. [3]

[c] – ν - stretching, δ - deformation, ρ_r – rocking, ρ_w – wagging, ρ_t - twisting, τ – torsional, ip – in-phase mode, op – out-of-phase mode

Table 6. Effect of complex formation on wavenumbers of ν(N-O) and ν(Pb-X) stretching modes computed at ZAPT2/SBKJC+(d) level in harmonic (Harm) and DPT2-VSCF (Anh) approximation.

Complex	$\Delta\nu$(N-O)[b]			$\Delta\nu_s$(Pb-X)[c]			$\Delta\nu_a$(Pb-X)[c]		
	Harm	Anh	Exptl[a]	Harm	Anh	Exptl[a]	Harm	Anh	Exptl[a]
PbF_2··NO	-11.7	15.8	16.4	-15.6	-14.0	-8.8	-14.5	-14.0	-8.5
PbF_2··ON	-28.5	-33.4		-8.1	-6.4		-7.6	-7.0	
$PbCl_2$··NO	-4.1	14.2		-9.1	-8.9		-8.8	-8.6	
$PbCl_2$··ON	-25.8	-30.7		-4.2	-3.9		-3.8	-3.5	
$PbBr_2$··NO	-1.5	14.6		-1.0	-3.0		-6.4	-6.3	
$PbBr_2$··ON	-26.2	-28.0		-2.8	-3.1		-3.0	-3.1	
PbI_2··ON	-25.5	-30.4		-1.2	-1.4		-2.4	-2.1	

[a] – Ar matrix spectra Ref. [3]

[b] - $\Delta\nu$(N-O)= $\nu(N\text{-}O)_{complex}$ - ν(N-O); anharmonic shifts computed from wavenumbers corrected for single mode (diagonal) anharmonicity

[c] - $\Delta\nu$(Pb-X)= $\nu(Pb\text{-}X)_{complex}$ - $\nu(Pb\text{-}X)_{halide}$

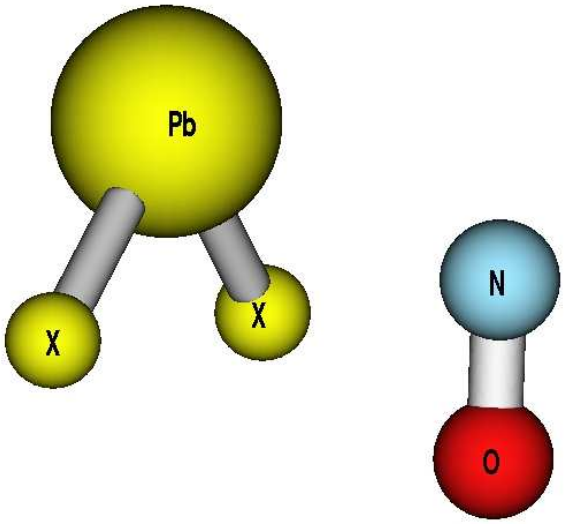

Figure 1. Equilibrium geometry of $PbX_2 \cdot\cdot NO$ complexes computed at ZAPT2/SBKJC+(d) level (Molden [44] drawing).

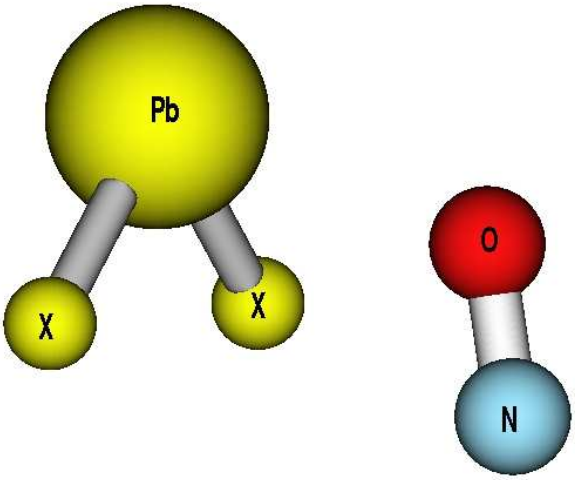

Figure 2. Equilibrium geometry of $PbX_2 \cdot\cdot ON$ complexes computed at ZAPT2/SBKJC+(d) level (Molden [44] drawing).

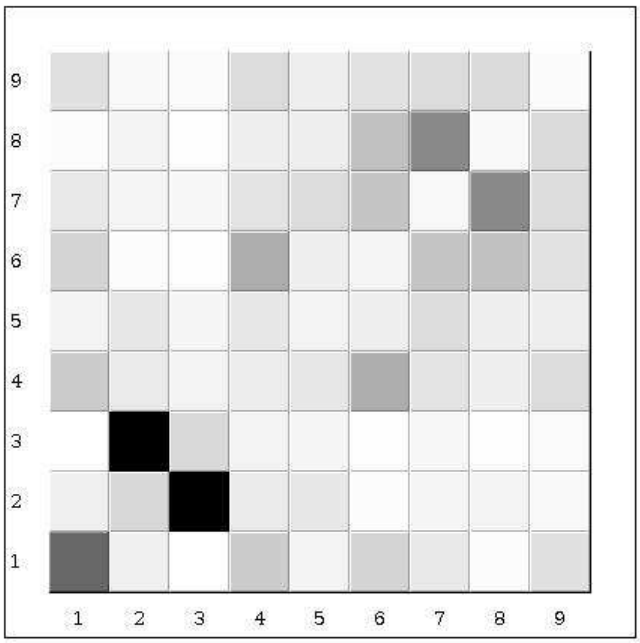

Figure 3. Two-dimensional mapping of $V_{i,j}^{coup}(Q_i , Q_j)$ mode coupling potential of $PbF_2 \cdot\cdot NO$ at ZAPT2/SBKJC+(d) level. Modes are labeled in the order of decreasing harmonic wave number (first column of Table 2) and the relative strength of the potential is coded in shades of gray (0, white and 255, black).

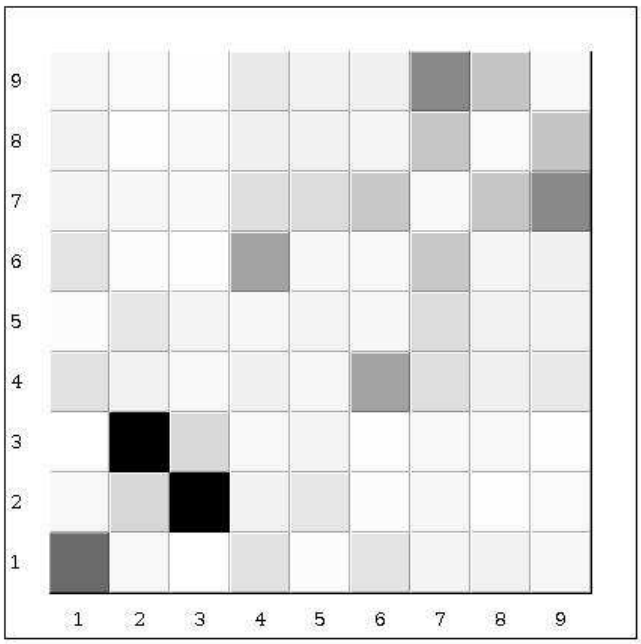

Figure 4. Two-dimensional mapping of $V_{i,j}^{coup}(Q_i , Q_j)$ mode coupling potential of PbF_2··ON at ZAPT2/SBKJC+(d) level. Modes are labeled in the order of decreasing harmonic wave number (first column of Table 2) and the relative strength of the potential is coded in shades of gray (0, white and 255, black).